

Active coherent beam combining of 1.55 μm pulsed fiber lasers based on intrapulse sampling

Zhen Liu (刘贞)^{1,2}, Yongke Zhang (张永科)¹, Qihao Shen (沈琪皓)^{1,2*}, Xingkai He (何幸锴)^{1,2}, Dingfu Zhou (周鼎富)^{1,2}, Liangyou Duan (段良友)^{1,2}, and Siyin Liu (刘思吟)^{1,2}

¹Southwest Institute of Technical Physics, Chengdu 610041, China

²Lidar and Device laboratory of Sichuan, Chengdu 610041, China

*Corresponding author: shen_qihao@163.com

Received December 1, 2024 | Accepted January 9, 2025 | Posted Online May 30, 2025

This study presents active coherent beam combining (CBC) of a pulsed laser based on sampling the intrapulse evaluation function. By precisely controlling the trigger sequence of an analog-to-digital converter, the fixed time point of the pulse light is sampled as an evaluation function for CBC. The active CBC of two fiber amplifiers with a 500 ns pulse width and a 10 kHz repetition rate is experimentally demonstrated by applying a hill-climbing algorithm. The residual phase error is approximately $\lambda/27$. A coherent Doppler wind lidar (CDWL) based on CBC light source is verified. The experimental results verify the feasibility of using the pulsed CBC to improve the pulse energy of a CDWL without degrading performance.

Keywords: single-frequency fiber laser; pulsed coherent beam combining; coherent Doppler lidar; active phase control.

DOI: [10.3788/COL202523.060605](https://doi.org/10.3788/COL202523.060605)

1. Introduction

Coherent Doppler wind lidars (CDWLs) have been widely applied in aviation security^[1], climate modeling^[2], wind-farm project optimization, and other fields. 1.55 μm single-frequency fiber lasers with low noise, narrow linewidth, high beam quality, and high integration have become primary light sources for CDWLs. For a high single-pulse energy output of single-frequency pulsed fiber lasers, the main oscillating power amplifier (MOPA) structure using erbium–ytterbium-doped fibers is well adapted^[3]. However, fiber amplifiers easily excite nonlinear effects owing to their small mode field area and high power density, and stimulated Brillouin scattering (SBS) is a nonlinear process with the lowest threshold because of approximately kilohertz linewidth of the light source, limiting the peak power of the output lasers^[4–6]. Coherent beam combining (CBC) allows the combination of the energy of serial fiber amplifiers and output light sources while simultaneously maintaining the linewidth, beam quality, and polarization degree of the subbeam. This is an important method to overcome the bottleneck of single-frequency pulsed fiber laser energy^[7,8].

In a continuous CBC system, the phase compensation direction is determined by the sampling intensity value. However, the intensity modulation of the pulsed laser affects the judgment of the phase difference^[9–11]. Therefore, extracting the phase difference between each subbeam is a research focus for pulsed CBC systems. Currently, for low-repetition (< 100 kHz) pulsed CBC adopted in CDWLs, the phase lock is mainly achieved using a

low-power continuous wave light leak. Lombard *et al.* realized two-element CBC of nanosecond pulsed lasers with a 10 kHz repetition rate by applying the dithering algorithm^[7]. Su *et al.* realized two-element CBC of hundred-nanosecond pulsed lasers with a 5 kHz repetition rate at a combining efficiency of 89%^[12]. Fan *et al.* simultaneously accomplished phase locking and tilt correction and realized two-element CBC of pulsed fiber lasers with a repetition frequency of 15 kHz and a pulse width of 100 ns at a combining efficiency of 95% via the stochastic parallel gradient descent (SPGD) algorithm^[13]. Nonetheless, the pulsed CBC system using a CW as the beacon signal is complex. For CDWL, an emission source with CW light results in additional optical noise and a low signal-to-noise ratio (SNR).

This study presents the active CBC of a pulsed laser based on sampling the intrapulse evaluation function for CBC with low repetition, avoiding a CW light leakage. Meanwhile, the pulsed CBC system based on intrapulse sampling is simpler than using a low-power CW light leak. Phase locking is accomplished by directly sampling a fixed time point of the pulsed light as the feedback signal of the active phase control evaluation function. The experimental results demonstrated that the pulsed CBC technology is applicable for improving the pulse energy of a CDWL without degrading performance.

2. Principle and Method

The experimental setup of the active pulsed CBC is shown in Fig. 1, which includes part of the CBC optical path and pulsed

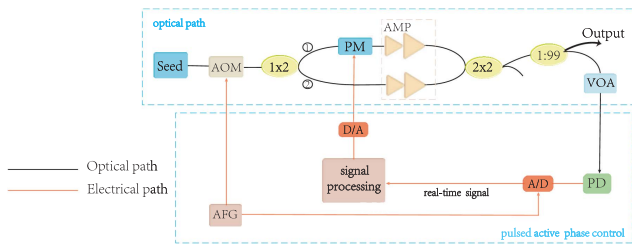


Fig. 1. Experimental setup for active pulsed CBC.

active phase control. For the CBC optical path, a 1550 nm distributed Bragg reflector (DBR) seed laser with a power of 10 mW is modulated using an acoustic-optic modulator (AOM) to produce 500 ns pulses at a repetition frequency of 10 kHz. The output of the pulsed laser is then split into two arms using a 50/50 coupler. One arm is coupled to a phase modulator (PM) with a half-wave voltage of 4 V, which is controlled to achieve phase synchronization. The two arms are coupled to a two-stage fiber amplifier (AMP). The first stage is an Er-doped fiber amplifier, and the second stage is an ErYb-co-doped fiber amplifier. The average laser power in the two channels is 70 mW and the single-pulse energy is 7 μ J. The amplified outputs of the two laser channels are combined using a 2×2 coupler. Then the combined beam is split into two arms using a 1/99 splitter. The port with a power of 99% is the output arm and the 1% is the feedback arm.

In pulsed active phase control, to generate the phase-control signal in the pulsed active phase controller, the feedback arm is attenuated to an appropriate range using an attenuator (VOA) and connected to a photodetector (PD). The intensity detected by the PD is defined as evaluation function J and will be used in the hill-climbing algorithm, which was employed to make the evaluation function J and the laser power of output beam to be at a maximum. The phase control processes are as follows:

- 1) Set phase control voltage u , then obtain the corresponding evaluation function J ; generate disturbance voltage $\pm\delta u$;
- 2) Compare J with J_{th} . If $J > J_{th}$, keep phase control voltage unchanged and acquire real-time evaluation function to compare with J_{th} ; If $J < J_{th}$, carry out step 3) of the procedure;
- 3) Set phase control voltage $u + \delta u$; then obtain the corresponding evaluation function $J(u + \delta u)$;
- 4) Compare $J(u + \delta u)$ with $J(u)$. If $J(u + \delta u) > J(u)$, apply the control voltages with $+\delta u$ to the PM in the next disturbances, return to step 2) of the procedure; if $J(u + \delta u) < J(u)$, apply the control voltages with $-\delta u$ to the PM in the next disturbances, then obtain the corresponding evaluation function $J(u - \delta u)$;
- 5) Compare $J(u - \delta u)$ with $J(u)$. If $J(u - \delta u) > J(u)$, apply the control voltages with $-\delta u$ to the PM in the next disturbances; repeat procedures 2) to 5).

The above phase control processes require real-time acquisition of evaluation functions J . However, the signal light intensity cannot always be obtained using pulsed lasers. Therefore,

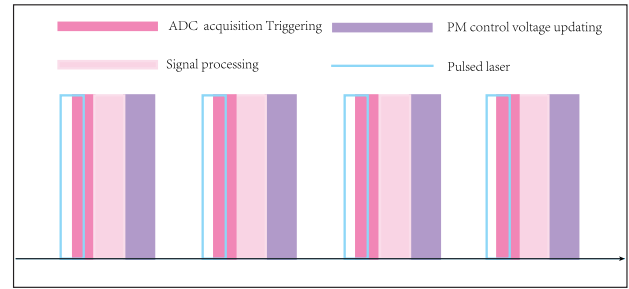


Fig. 2. Control timing diagram of pulsed CBC.

the timing of the trigger acquisition is synchronized with the AOM driving signal to acquire the evaluation function J and achieve feedback control. The control timing diagram of the pulsed CBC is shown in Fig. 2. By controlling the timing of the AOM driving and analog-to-digital converter (ADC) trigger signal using an arbitrary function generator (AFG), the pulsed signal can be sampled at a fixed point of the pulse light to avoid sampling errors caused by the nonrectangular pulse waveform after the gain of the fiber amplifier. Since the pulse width is on the order of hundreds of nanoseconds that need accurate sampling, the AFG and ADC with a 2.5 GHz sampling rate are used in Fig. 1. Then, the phase control voltage is judged by the hill-climbing algorithm. According to the hill-climbing phase control processes, the direction of voltage control is determined by comparing the evaluation function before and after applying the disturbance voltage. For the pulsed CBC, the comparison is the fixed-point acquisition value of adjacent pulses.

3. Results of Pulsed CBC

In the pulsed CBC system based on intrapulse sampling, two factors can introduce additional perturbations in the acquisition of the evaluation function J . First, during the subbeam amplification, pump disturbances, amplification of spontaneous emission, and other factors can cause intensity noise, leading to instability in the subbeam waveform. Second, the delay of electronic components limits the accuracy of sampling timing, and there will be errors in the acquisition of nonrectangular pulse waveforms. Before implementing the pulsed CBC, we sampled the intensity of the two pulsed subbeams at the fixed time point to judge the effects of waveform instability and acquisition timing accuracy on J , as shown in Fig. 3. The fixed time point is set at

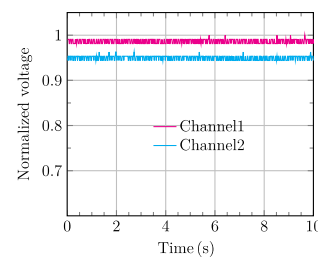


Fig. 3. Sampled intensity of the two pulsed subbeams at the fixed time point.

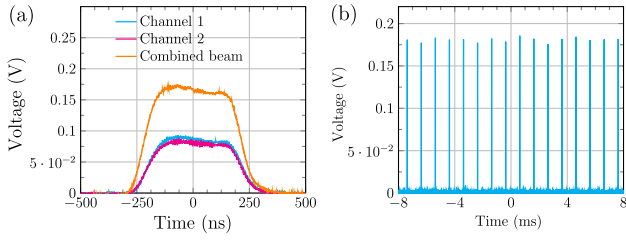


Fig. 4. Results. (a) Pulse shapes of two channels and combined beam in one cycle; (b) pulse shape of combined beam in multicycle.

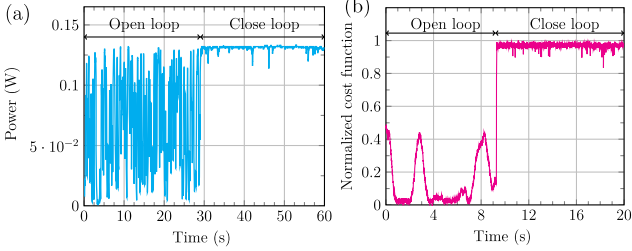


Fig. 5. Results. (a) Output powers in open loop and closed loop; (b) normalized cost functions in open loop and closed loop.

the flatter middle part of the pulse waveform. The fluctuation of the sampled values from the two subbeams is less than 2%, and the disturbance to J is small compared to δu . Therefore, the influence on the phase control processes can be disregarded.

The temporal profiles of the amplified and combined beams are shown in Fig. 4. The consistency of the two fiber amplifiers is ensured to the maximum possible extent via the fabrication process, including the gain and fiber length (difference of less than 0.2 m). Therefore, the two pulsed lasers overlap in the time domain, and the combined pulse waveforms are consistent with those of the subbeam. Figure 5 shows the changes in the power and normalized cost function J before and after loop closure. In the open-loop state, the output power fluctuates owing to the impact of vibration and thermal noise in the system, which results in a random phase jitter. By implementing a phase-locking feedback loop, the output power is stabilized at approximately 132 mW. A residual phase error of $\lambda/27$ is evaluated by Eq (1),

$$\varphi_{\text{RMS}} = 2 \sqrt{\frac{\Delta V_{\text{RMS}}}{V_{\text{max}}}} \quad (1)$$

4. Application of Pulsed CBC in CDWL

Pulsed CBC can be applied to improve the emission energy. According to the lidar equation as shown in Eq. (2)^[14],

$$P_{\text{rec}} = \frac{E \cdot \eta_r \cdot \eta_{\text{tran}} \cdot \beta \cdot c \cdot A_{\text{rec}} \cdot T^2}{2L^2} \propto \frac{E}{L^2}, \quad (2)$$

where P_{rec} is the power of the echo signal, E is the energy of the emission source, L is the detection range, η_r is the receiving

efficiency, η_{tran} is the transmission efficiency, T is the single-way atmospheric transmittance, β is the atmospheric backscatter coefficient, α is the atmospheric extinction coefficient, A_{rec} is the effective receiving area of the antenna, and c is the speed of light. It can be seen that echo power is proportional to the emission energy. To verify the feasibility of the pulsed CBC in CDWLs, we compared the CDWL measurement results of the pulsed CBC with those of a conventional single-beam pulsed light source.

The setup of the CDWL based on the pulsed CBC is shown in Fig. 6. The circulator (CIR) separates the transmitted pulsed laser and the continuous optical atmospheric backscatter signal in opposite directions. The output light source is sent to the atmosphere via port 2 of the CIR. The transceiver system adopts an integrated configuration and uses a 100 mm aperture telescope. The optical atmospheric backscatter signal will be received by the telescope. In the receiving system, the backscattered signal is mixed with a local oscillator light using a 2×2 coupler and beats on a balanced photodetector (BPD), realizing coherent detection.

Triple light sources are compared, including single-beam with 5.4 μJ (source A, listed in Table 1), single-beam with 10.8 μJ (source B, listed in Table 1), and two-beam CBC light source with 10.8 μJ (source C, listed in Table 1). Figure 7 shows the narrowband SNR of CDWL for three different light sources. Given the higher power, source C exhibits a 4 dB higher SNR than source A. Meanwhile, the SNR of source C is comparable to that of source B.

Figure 8 shows the wind velocity profiles of the lidar for the three different light sources. Figure 8(a) denotes source A, Fig. 8(b) denotes source B, and Fig. 8(c) denotes source C. According to Eq. (2), the energy of a single pulse increases by

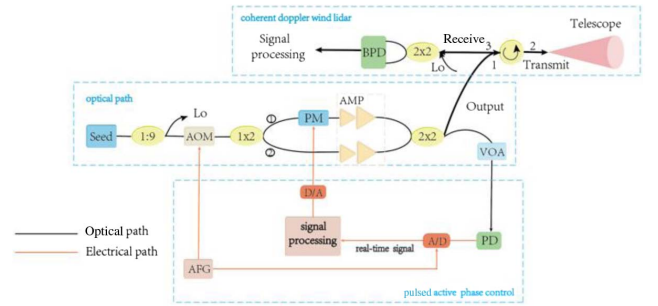


Fig. 6. Setup for coherent Doppler wind lidar based on pulsed CBC.

Table 1. Parameters of Three Light Sources.

Source	Value (μJ)	Illustrate
A	5.4	single-beam
B	10.8	single-beam
C	10.8	two-beam CBC

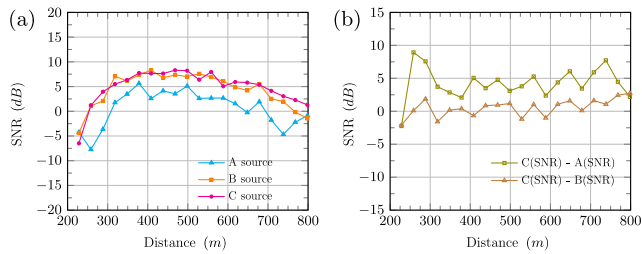


Fig. 7. Results of SNR. (a) Average SNR; (b) SNR difference.

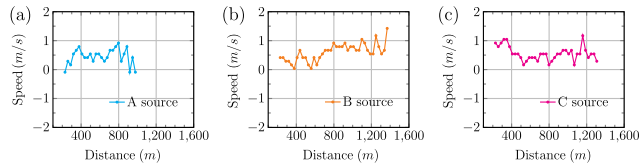


Fig. 8. Wind velocity profiles. (a) Source A; (b) source B; (c) source C.

a factor of 2, and the detection range can be increased by $\sqrt{2}$ times. In Fig. 8, the steady wind speed test distance range for the pulsed CBC and single-beam light with $10.8 \mu\text{J}$ is 1300 m, and single-beam light with $5.4 \mu\text{J}$ is 950 m. Compared to the $5.4 \mu\text{J}$ single beam, the detection range of the CDWL using the pulsed CBC is increased by 1.36 times. Overall, the CDWL performance of the CBC laser beam and single laser beam at equal energy is comparable, which verifies the feasibility of using the pulsed CBC to improve the pulse energy of a CDWL without degrading performance.

5. Discussion

The pulsed CBC based on intrapulse sampling requires accurate acquisition timing control, and a narrower pulse width requires higher acquisition timing precision. Currently, electronic components, such as A/D chips, are limited to the gigahertz range, limiting the accuracy of acquisition timing to the nanosecond level. Therefore, this scheme is more suitable for pulsed CBC systems with pulse widths exceeding 100 ns. Currently, CDWLs with all-fiber structured light sources and detection ability exceeding 10 km, the pulse widths are designed to be 200 ns–1 μs to achieve the requirement of submillijoule-level emission energy^[15]. Therefore, the above emission source can serve as a subbeam in an amplification array, compatible with the pulsed CBC technique based on intrapulse sampling. The fiber coupler with limited power handling is used as the beam combiner in Fig. 1 and can be replaced by a polarization coherent beam combiner with higher power handling. Then, on the current output level of the $1.5 \mu\text{m}$ single-frequency pulsed fiber laser, the multibeam CBC can be achieved to breakthrough output single pulse energy up to the millijoule level and coherent detection at a longer distance.

6. Conclusion

In conclusion, an active CBC of pulsed laser based on sampling the intrapulse evaluation function is demonstrated. By precisely controlling the trigger sequence of the ADC, the fixed time point of the pulse light is sampled as the evaluation function. Then the hill-climbing algorithm is applied to correct the phase errors. In the experiment, the active CBC of two fiber amplifiers with a pulse width of 500 ns, a repetition rate of 10 kHz, and a phase error of $\lambda/27$ has been achieved. Furthermore, the applicability of the pulsed CBC in the system is verified. Experimental results show that the CDWL performance of the CBC laser beam and the single laser beam at equal energy are comparable, which verifies the feasibility of using the pulsed CBC to improve the pulse energy of a CDWL without degrading performance. In future work, the single-frequency pulse fiber laser based on the current output level can be combined with the pulsed CBC technology. This approach can overcome the limitations of output energy and provide a single-frequency laser source with higher pulse energy for lidar, atmospheric remote sensing, spectral analysis, and other remote coherent detection fields with high spatiotemporal accuracy.

Acknowledgements

This work was supported by the Foundation of Lidar and Device Laboratory, Sichuan Province, China and the Basic Military Research Institutes Steadily Support Special Projects.

References

1. R. Stephan, I. Smalikho, and F. Köpp, "Characterization of aircraft wake vortices by airborne coherent Doppler lidar," *J. Aircraft* **44**, 799 (2007).
2. D. T. Michel, A. Dolfi-Bouteyre, D. Goular, *et al.*, "Onboard wake vortex localization with a coherent $1.5 \mu\text{m}$ Doppler LIDAR for aircraft in formation flight configuration," *Opt. Express* **28**, 14374 (2020).
3. P. Wan, J. Liu, L.-M. Yang, *et al.*, "Low repetition rate high energy $1.5 \mu\text{m}$ fiber laser," *Opt. Lett.* **19**, 18067 (2011).
4. G. Canat, W. Renard, E. Lucas, *et al.*, "Eyesafe high peak power pulsed fiber lasers limited by fiber nonlinearity," *Opt. Fiber Technol.* **20**, 678 (2014).
5. J. Hansryd, F. Dross, M. Westlund, *et al.*, "Increase of the SBS threshold in a short highly nonlinear fiber by applying a temperature distribution," *J. Lightwave Technol.* **19**, 1691 (2001).
6. L. V. Kotov, M. E. Likhachev, M. M. Bubnov, *et al.*, "Record-peak-power all-fiber single-frequency 1550 nm laser," *Laser Phys. Lett.* **11**, 095102 (2014).
7. L. Lombard, A. Azarian, K. Cadoret, *et al.*, "Coherent beam combination of narrow-linewidth $1.5 \mu\text{m}$ fiber amplifiers in a long-pulse regime," *Opt. Lett.* **36**, 523 (2011).
8. L. Lombard, M. Valla, C. Planchat, *et al.*, "Eyesafe coherent detection wind lidar based on a beam-combined pulsed laser source," *Opt. Lett.* **40**, 1030 (2015).
9. P. Ma, P. Zhou, Y. Ma, *et al.*, "Coherent polarization beam combining of four fiber amplifiers in 100 ns pulsed-regime," *Opt. Laser Technol.* **47**, 336 (2013).
10. F. Guichard, M. Hanna, L. Lombard, *et al.*, "Two-channel pulse synthesis to overcome gain narrowing in femtosecond fiber amplifiers," *Opt. Lett.* **38**, 5430 (2013).
11. J. Zhang, J. Cao, Q. Hao, *et al.*, "Window filtering algorithm for a low repetition rate pulsed laser coherent combination system," *Appl. Opt.* **61**, 8484 (2022).
12. R. Su, P. Zhou, X. Wang, *et al.*, "Actively coherent beam combining of two single-frequency 1083 nm nanosecond fiber amplifiers in low-repetition-rate," *IEEE Photonics Technol. Lett.* **25**, 1485 (2013).

13. F. Zou, J. Zuo, C. Geng, *et al.*, "Indirectly coherent beam combining of pulsed lasers based on active control of continuous carrier," *Opt. Eng.* **60**, 066111 (2021).
14. F. Takashi and F. Tetsuofukuch, *Laser Remote Sensing* (CRC Press Taylor & Francis Group, 2005).
15. R. William, G. Didier, V. Matthieu, *et al.*, "Beyond 10 km range wind-speed measurement with a 1.5 μm all-fiber laser source," in *Proceedings of the 2014 Conference on Lasers and Electro-Optics (CLEO) - Laser Science to Photonic Applications* (2014).